Catalysis Science & Technology

ROYAL SOCIETY OF CHEMISTRY

COMMUNICATION

View Article Online
View Journal | View Issue

Check for updates

Cite this: *Catal. Sci. Technol.*, 2025, 15, 669

Received 18th October 2024,
Accepted 30th December 2024

DOI: 10.1039/d4cy01244e

rsc.li/catalysis

Rational design of stainless steel self-catalytic reactors for CO_2 methanation: extending from metal powder to 3D-printed reactors†

Hyo-Jin Kim,[a] Kohsuke Mori, *[abc] Takayoshi Nakano [ab] and Hiromi Yamashita [ac]

A design framework for metal 3D-printed self-catalytic reactors (3D SCRs) using stainless steel (STS) has been demonstrated. The surface functionalization of STS was achieved through a two-step dealloying process, which is first optimized on metal powder precursor, and then successfully extended to STS 3D SCRs as a practical active catalyst for CO_2 methanation.

Introduction

The development of metal 3D-printed self-catalytic reactors (3D SCRs) represents a key innovation, combining additive manufacturing and catalytic systems to overcome challenges in the chemical engineering field.[1,2] The integration of the catalyst and reactor functions in 3D SCRs facilitates the catalyst development process, enabling a more direct transition from laboratory research to industrial implementation.[3] Moreover, it allows the fabrication of intricate geometrical configurations that are not achievable by conventional methods, thereby improving heat and mass transfer rates within the reactor.[4,5] This addresses several common issues observed in traditional packed-bed reactors, including the formation of hot and cold spots, pressure drops, and reactant maldistribution.[6–8]

The design of 3D SCRs hinges on two critical factors: geometric optimization and surface functionalization, both of which are essential for maximizing catalytic performance.[9,10] In the case of geometric optimization, computational fluid dynamics (CFD) technology facilitates the efficient design of structures, obviating the necessity for extensive experimental trials.[4] On the other hand, the process of surface functionalization remains a challenge due to the time-consuming and costly procedure, which involves repeatedly confirming the surface properties and catalytic activity of 3D-printed samples. We have previously demonstrated for the first time that selective electrochemical dissolution is a promising surface functionalizing strategy to transform an as-printed reactor using Hastelloy X into an active Ni-based SCR for CO_2 methanation.[10] However, the lack of standardized methodologies complicates this challenge, and a more simple approach is desired.

Hence, in this study, we present a design strategy that optimizes surface functionalization from the metal powder precursor to the final 3D SCRs. The use of powdered samples in the optimization process prior to fabrication of 3D SCRs allows for a reduction in the time and effort required for sample preparation and functionalization condition selection. The versatile stainless steel (STS, Fe–Cr–Ni alloy) was selected for the CO_2 methanation reaction, and a two-step dealloying method was employed for surface functionalization (Scheme 1). To investigate the relationship between the scan speed and catalytic activity, STS 3D SCRs were fabricated at two different laser scan speeds (800 mm s^{-1} and 1200 mm s^{-1}) using gas atomized (GA) STS316L powder and selective laser melting (SLM) (Fig. S1†). The details are in the ESI.† All resulting materials were characterized together with a catalytic activity test, SEM-EDS, XRD, and XPS.

Results and discussion

To prepare the catalyst for CO_2 methanation, it is essential for Ni or Ni–Fe species to be exposed on the surface to activate H_2 and CO_2.[10,11] However, the as-produced STS 3D-printed reactors (3D SCRs) and powder were predominantly covered by a mixture of inactive Cr and Fe oxides (Fig. S2†). To selectively leach Cr and Fe while preserving active Ni species, hydrothermal treatment of STS powder in a concentrated caustic soda solution (50 wt% NaOH) was conducted as an initial step. STS 316L, containing over 55–60 atomic percent reactive species (Fe and

[a] *Division of Materials and Manufacturing Science, Graduate School of Engineering, Osaka University, 2-1 Yamadaoka, Suita, Osaka 565-0871, Japan. E-mail: mori@mat.eng.osaka-u.ac.jp*
[b] *Anisotropic Design & Additive Manufacturing Research Center, Osaka University, 2-1, Yamadaoka, Suita, Osaka 565-0871, Japan*
[c] *Innovative Catalysis Science Division, Institute for Open and Transdisciplinary Research Initiatives (ICS-OTRI), Osaka University, Suita, Osaka 565-0871, Japan*
† Electronic supplementary information (ESI) available. See DOI: https://doi.org/10.1039/d4cy01244e

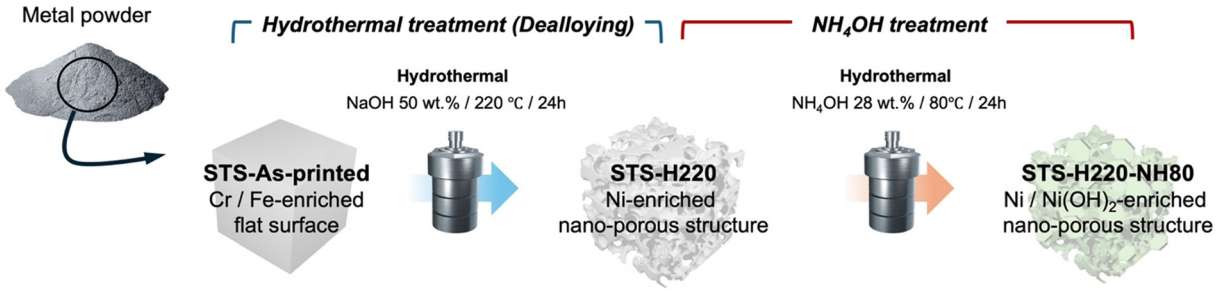

Scheme 1 Two-step surface functionalization method of STS metal powder and 3D SCRs.

Cr), meets the geometric parting limit for chemical dealloying, allowing the retention of noble Ni species in the hot caustic solution.[12,13]

The catalytic performance for CO_2 methanation before and after the initial hydrothermal treatment is presented in Fig. 1. Prior to dealloying, the as-printed STS powder exhibited minimal catalytic activity (~0.1% CO_2 conversion). After hydrothermal treatment in 50 wt% NaOH (STS-H220), the powder surface was dealloyed, achieving a 3.7% CO_2 conversion. In comparison, a Ni alloy (Ni–21Cr–18Fe–8Mo at%) that is insufficient for dealloying due to not meeting the geometric parting limit exhibited 9.1-fold lower catalytic performance than STS-H220, confirming the potential of the dealloying process for optimizing catalytic activity (Fig. S3†). Nevertheless, the selectivity of CH_4 remained low at 16.3%, prompting further refinement treatment.

Hence, as a second step, the dealloyed STS at 220 °C in 50 wt% NaOH (STS-H220) was treated with ammonia solution (NH_4OH) to eliminate residual Fe and Cr oxides and further expose the active Ni sites for CO_2 methanation. Among various NH_4OH treatment conditions, a temperature of 80 °C was found to be optimal and denoted as STS-H220-NH80, yielding a 21.8% CO_2 conversion and 92.4% CH_4 selectivity, with an improvement of 218 times over the STS raw powder (Fig. 1).

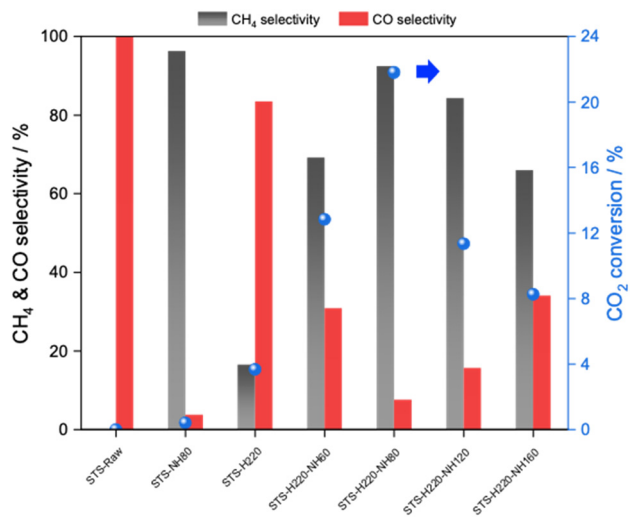

Fig. 1 CO_2 methanation performance of STS powder samples before and after each treatment step. Reaction conditions: T = 300 °C, P = 1 bar, flow rate = 20 mL min^{-1}, reaction gas = $H_2/CO_2/N_2$ = 64/16/20.

Additionally, the catalytic performance of STS-H220-NH80 was stable even after a 1000 minute long-term test at 300 °C, highlighting the reliability of this surface functionalization method (Fig. S4†). The minor CO selectivity is attributed to the residual Fe oxide formed during dealloying and washing processes (Fig. S5†).

Based on the results obtained from the STS metal powder precursor, the same surface functionalization procedure was applied to the 3D SCRs. A scan speed of 1200 mm s^{-1} was

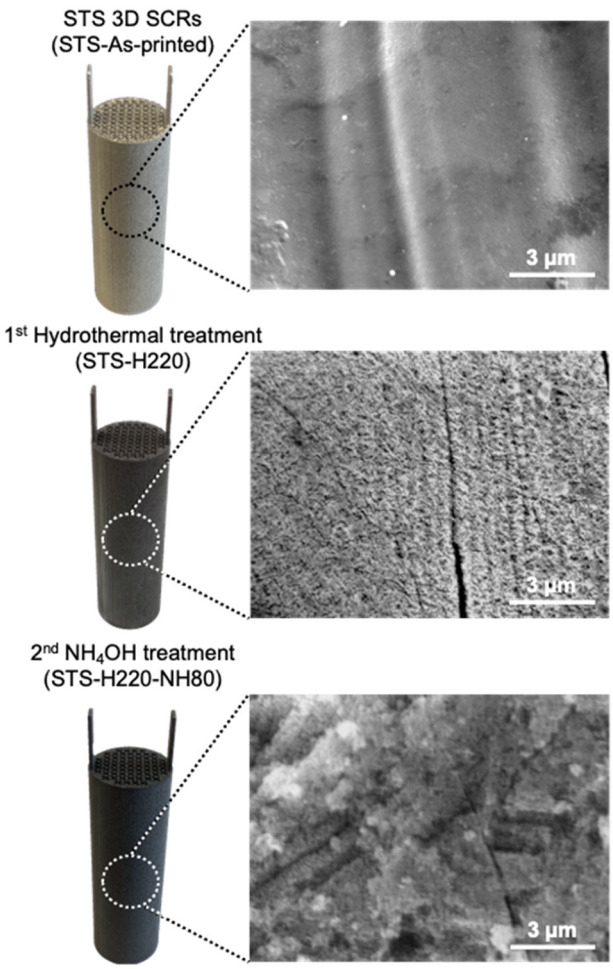

Fig. 2 Photographs and SEM images of STS 3D SCRs before and after each treatment step. The scan speed for the 3D printing process is 1200 mm s^{-1}.

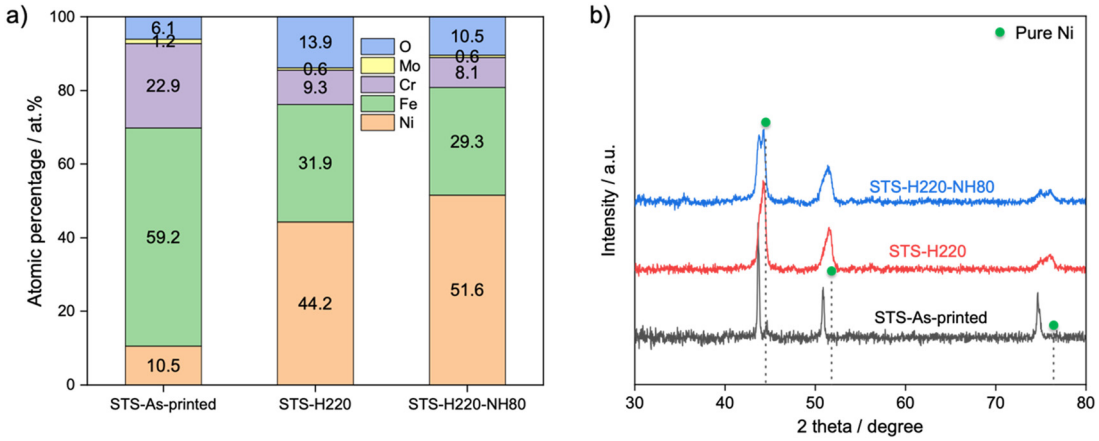

Fig. 3 a) EDS quantification and b) XRD profiles of STS 3D SCRs before and after each treatment step.

utilized for the 3D SCR samples. Fig. 2 illustrated the uniform color change of the external 3D SCRs before and after each treatment step, implying surface property transformation. SEM images show the development of a Ni-enriched nanoporous structure after the initial hydrothermal treatment (Fig. 2 and 3a). This nanoporous structure remained stable after the second NH_4OH treatment, transitioning to a finer morphology with an increase in the Ni content, reaching 51.6 at% as determined by EDS (Table S3† and Fig. 3a). XRD analysis showed a significant positive shift in peaks towards pure nickel after the first and second dealloying steps (Fig. 3b), supporting the formation of a Ni-enriched solid solution phase, which is consistent with SEM-EDS findings.[13,14] XPS measurements before and after each treatment confirmed that the surface composition evolved from being predominantly Cr (33.8 at%) and Fe (62.3 at%), which are inactive for CO_2 methanation, towards a Ni-enriched surface (49.6 at%), containing a mixture of metallic Ni, $Ni(OH)_2$, and NiOOH species (Fig. S2†).

Subsequently, the catalytic activity of dealloyed 3D SCRs fabricated with a scan speed of 1200 mm s^{-1} (v = 1200-H220-NH80) was evaluated across a temperature range of 200–400 °C (Fig. 4a). The v = 1200-H220-NH80 3D SCRs demonstrated high CO_2 methanation performance, achieving a CO_2 conversion rate of 78.5% and CH_4 selectivity of 99.9% at 350 °C, indicating the successful extension of the insight obtained in the metal powder optimization process to 3D SCRs.

Furthermore, the effect of different scan speeds in the 3D printing process on the catalytic activity of STS 3D SCRs was investigated after the optimized two-step dealloying process. The sample fabricated with a scan speed of 1200 mm s^{-1} (v = 1200-H220-NH80) showed 1.1 to 1.4 times higher catalytic activity compared to the 800 mm s^{-1} sample (v = 800 H220-NH80) (Fig. 4b). This difference is attributed to the influence of the scan speed, which is directly linked to the energy density of the scanning conditions (Table S2†). This energy density difference leads to variations in the crystal texture of

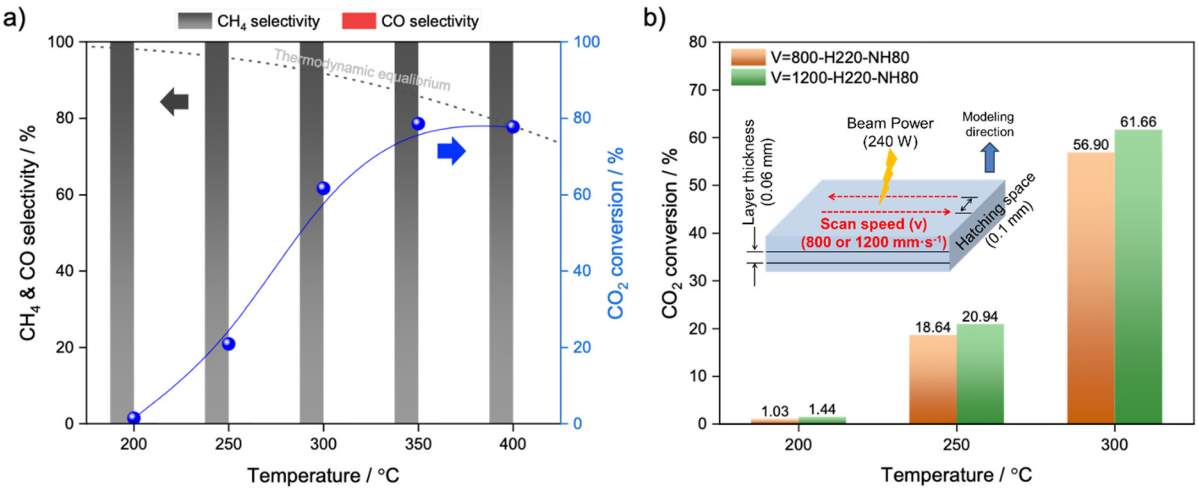

Fig. 4 a) Temperature-dependent CO_2 conversion with v = 1200-H220-NH80 and b) CO_2 methanation performance with different scan speeds. Reaction conditions: P = 1 bar, flow rate = 20 mL min^{-1}, reaction gas = $H_2/CO_2/N_2$ = 64/16/20.

the 3D-printed samples. The sample printed at ν = 1200, with a lower laser energy density compared to ν = 800, is expected to form finer grains, facilitating the dealloying of STS by increasing the number of active sites on the grains.[15–17]

Conclusions

In conclusion, STS 3D self-catalytic reactors (STS 3D SCRs) were successfully developed by extending the insight obtained with metal powder precursors to functional 3D-printed reactors. The two-step dealloying process, initially optimized using the metal powder, was effectively applied to the 3D SCRs, resulting in the significant enhancement of CO_2 methanation performance through the transformation of the STS surface into Ni-enriched species. Additionally, the influence of the scan speed on catalytic activity was demonstrated, highlighting the need for further detailed investigations to elucidate the relationship between the scan speed and 3D SCR performance optimization. This work presents a novel approach to designing 3D SCRs, offering a method that reduces both time and costs in the development process. Further studies for the effect of geometric structures and differences in the crystallographic texture properties induced by the different scan strategies are now under investigation.

Data availability

The data underlying this article are available in the article and in its online ESI.†

Author contributions

H. K. performed the sample preparation, calculation, and characterization, and wrote the manuscript with help from K. M. K. M. supervised the entire project and provided funding. T. N. helped with the preparation of the metal 3D printed reactor. H. Y. helped supervise the project. The manuscript was written through the discussion with all authors. All authors have given approval to the final version of the manuscript.

Conflicts of interest

There are no conflicts of interest to declare.

Acknowledgements

This work was financially supported by a project (Project no. JPNP14004, Grant Number: 24018730), commissioned by the New Energy and Industrial Technology Development Organization (NEDO). This work was also partly supported by CREST-Nanomechanics: Elucidation of macroscale mechanical properties based on understanding nanoscale dynamics for innovative mechanical materials (Grant Number: JPMJCR2194) from the Japan Science and Technology Agency (JST).

Notes and references

1 H. J. Kim, K. Mori, T. Nakano and H. Yamashita, *ChemCatChem*, 2024, **16**, 3–8.
2 X. Zhao, C. Karakaya, M. Qian, R. Zou, W. Zhang, Z. Lu, D. Maiti, A. Samanta, W. Wan, X. Liu, A. Tiplea, Y. Li, S. Cui, C. Wang, H. Lei, S. Bankston, S. Yilmaz, J. G. Chen and S. Ozcan, *Mater. Today Sustain.*, 2024, **26**, 100746.
3 Q. Wei, H. Li, G. Liu, Y. He, Y. Wang, Y. E. Tan, D. Wang, X. Peng, G. Yang and N. Tsubaki, *Nat. Commun.*, 2020, **11**, 4098.
4 W. Li, J. Ding, X. Chen, Y. Wang, X. Song and S. Zhang, *J. Mater. Chem. A*, 2023, **12**, 314–320.
5 G. Vilé, D. Ng, Z. Xie, I. Martinez-Botella, J. Tsanaktsidis and C. H. Hornung, *ChemCatChem*, 2022, **14**, e202101941.
6 B. Partopour and A. G. Dixon, *Ind. Eng. Chem. Res.*, 2019, **58**, 5733–5736.
7 N. Erfani, D. Symons, C. Fee and M. J. Watson, *Chem. Eng. Res. Des.*, 2024, **211**, 212–220.
8 T. A. Nijhuis, A. E. W. Beers, T. Vergunst, I. Hoek, F. Kapteijn and J. A. Moulijn, *Catal. Rev.:Sci. Eng.*, 2001, **43**, 345–380.
9 K. Mori, T. Fujita, H. Hata, H. J. Kim, T. Nakano and H. Yamashita, *ACS Appl. Mater. Interfaces*, 2023, **15**, 51079–51088.
10 H. J. Kim, K. Mori, T. Nakano and H. Yamashita, *Adv. Funct. Mater.*, 2023, **2303994**, 1–11.
11 H. L. Huynh, J. Zhu, G. Zhang, Y. Shen, W. M. Tucho, Y. Ding and Z. Yu, *J. Catal.*, 2020, **392**, 266–277.
12 K. Sieradzki, N. Dimitrov, D. Movrin, C. McCall, N. Vasiljevic and J. Erlebacher, *J. Electrochem. Soc.*, 2002, **149**, B370.
13 J. Deakin, Z. Dong, B. Lynch and R. C. Newman, *Corros. Sci.*, 2004, **46**, 2117–2133.
14 T. Ghaznavi, M. A. Bryk, S. Y. Persaud and R. C. Newman, *Corros. Sci.*, 2022, **197**, 110003.
15 J. Liu, Y. Song, C. Chen, X. Wang, H. Li, C. Zhou, J. Wang, K. Guo and J. Sun, *Mater. Des.*, 2020, **186**, 108355.
16 J. Akram, P. Chalavadi, D. Pal and B. Stucker, *Addit. Manuf.*, 2018, **21**, 255–268.
17 S. Gollapudi, *Corros. Sci.*, 2012, **62**, 90–94.

